

## Enhanced piezoelectric response from barium strontium titanate multilayer films

R. Nath, S. Zhong, S. P. Alpay, and B. D. Huey<sup>a)</sup>

*Materials Science and Engineering Program and Institute of Materials Science, University of Connecticut, Storrs, Connecticut 06269, USA*

M. W. Cole

*Weapons and Materials Research Directorate, Active Materials Research Group, U.S. Army Research Laboratory, Aberdeen Proving Ground, Maryland 21005, USA*

(Received 13 July 2007; accepted 27 November 2007; published online 7 January 2008)

Multilayered and homogeneous thin films of  $\text{Ba}_x\text{Sr}_{1-x}\text{TiO}_3$  (BST) were grown on Pt-coated Si substrates via metal-organic solution deposition. The multilayer 220 nm thick BST heterostructure consisted of  $\text{Ba}_{0.60}\text{Sr}_{0.40}\text{TiO}_3$ ,  $\text{Ba}_{0.75}\text{Sr}_{0.25}\text{TiO}_3$ , and  $\text{Ba}_{0.90}\text{Sr}_{0.10}\text{TiO}_3$ . A single composition 220 nm thick  $\text{Ba}_{0.60}\text{Sr}_{0.40}\text{TiO}_3$  was also grown for comparison. The piezoelectric properties were measured using piezoresponse force microscopy. There is approximately a 50% improvement in the piezoelectric response of the multilayered heterostructure compared to the homogeneous sample, with some spatial inhomogeneity. This enhancement can be attributed to the internal potential that arises from the polarization gradient and the commensurate built-in strain in the multilayer sample. © 2008 American Institute of Physics. [DOI: 10.1063/1.2825287]

Ferroelectric (FE) multilayer and functionally graded heterostructures have attracted considerable attention in recent years due to their interesting properties and potential device applications.<sup>1–6</sup> Most notably, these materials exhibit an enhanced spontaneous polarization,<sup>7</sup> huge effective pyroelectric response,<sup>8</sup> large piezoelectric strains,<sup>9</sup> and, if the polarization is systematically graded, a translation of the ferroelectric hysteresis loop along the polarization axis in an otherwise conventional hysteresis graph when driven by a symmetric period potential.<sup>10</sup> Furthermore, significant improvements in the dielectric permittivity and tunability were reported in  $\text{PbTiO}_3$ – $\text{Pb}_x\text{La}_{1-x}\text{TiO}_3$  and  $\text{BaTiO}_3$ – $\text{SrTiO}_3$  superlattices.<sup>2,4</sup> Recent results show that  $\text{Ba}_x\text{Sr}_{1-x}\text{TiO}_3$  (BST) multilayer heterostructures display high dielectric tunability with minimal temperature dependence from  $-10$  to  $90$  °C.<sup>11</sup>

Large piezoelectric strains can be expected from multilayer or graded FEs with systematic variations in the polarization due to an internal electrostatic potential that arises from the polarization gradient and the commensurate built-in strain field. Our recent theoretical results on the piezoelectric response of graded FEs (Ref. 9) indicate that these heterostructures may be as effective as reduced and internally biased oxide wafer<sup>12</sup> (RAINBOW™) and (thin unimorph driver) (THUNDER™) ceramics.<sup>13</sup> These are essentially bilayers consisting of a piezoelectric ceramic bonded to a cermet or a metal layer and the high displacement is the result of a built-in nonlinear stress field due to the thermal expansion mismatch between the layers. However, unlike these composites, there exists a built-in potential in polarization graded FEs, which may lead to the development of self-biased transducers. In this letter we report a 50% improvement in the piezoelectric response of multilayered BST films fabricated by metal-organic solution deposition (MOSD) over homogeneous BST films when measured via piezoresponse force microscopy (PFM).

Both multilayered [Fig. 1(a)] and homogeneous [Fig. 1(b)] thin films of BST were fabricated on Pt-coated high resistivity Si substrates (Pt/Si) via the industry standard MOSD technique using carboxylate-alkoxide precursors. The detailed description of the MOSD precursor solution preparation and film deposition technique was reported previously.<sup>14</sup> The multilayer heterostructure consisted of three distinct compositional layers (with  $\sim 220$  nm total thickness and with each layer  $\sim 70$  nm);  $\text{Ba}_{0.60}\text{Sr}_{0.40}\text{TiO}_3$  (BST60/40),  $\text{Ba}_{0.75}\text{Sr}_{0.25}\text{TiO}_3$  (BST75/25), and  $\text{Ba}_{0.90}\text{Sr}_{0.10}\text{TiO}_3$  (BST90/10) which were sequentially deposited onto the Pt/Si substrates. A multi-annealing process was utilized during the multilayer thin film process. The protocol comprised depositing of three coatings of each distinct composition layer (i.e., BST60/40, BST75/25, and BST90/10), onto the Pt/Si substrate, whereby after each individual spin-on film coating the sample was pyrolyzed at  $350$  °C for 10 min and, subsequently, postdeposition annealed at  $750$  °C for 60 min. in flowing oxygen. Therefore, the multilayer thin film was exposed to three postdeposition anneals at  $750$  °C, such that each distinct layer composition was fully crystallized prior to the deposition of the next compositional layer. As a reference, a uniform single composition 220 nm thick BST60/40 film was also fabricated using the same MOSD technique but only subjected to a single postannealing.

The multilayered heterostructure and the homogeneous films were characterized using x-ray diffraction, scanning electron microscope, and Rutherford backscattering spectrometry. It was found that both samples are polycrystalline

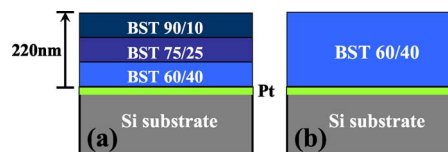


FIG. 1. (Color online) Schematic configurations of (a) the multilayer graded sample and (b) the homogeneous BST film.

<sup>a)</sup> Author to whom correspondence should be addressed. Electronic mail: bhuey@ims.uconn.edu.

with no apparent texture and do not contain secondary phases. The multilayer film consists of distinct three layers with designated compositions. The dielectric permittivity, loss, and tunability were measured as a function of temperature. At room temperature, a small-signal relative dielectric permittivity of 360 with a dissipation factor of 0.012 and a dielectric tunability of 65% at 444 kV/cm were obtained. These properties exhibited minimal dispersion as a function of temperature ranging from 90 to  $-10$  °C.<sup>11</sup> A detailed analysis of the synthesis method, characterization, and electrical measurements are presented elsewhere.<sup>15</sup>

The experimental setup for the PFM measurements included (1) MFP-3D™ stand alone atomic force microscope, (2) conductive diamond coated tips with apex radius of 50–150 nm and force constant of 30–40 N/m, (3) Agilent 33259A 80 MHz function waveform generator, and (4) Stanford research systems, model 844 rf lock-in amplifier. PFM is an atomic force microscopy (AFM) related technique, which has been routinely used to image and characterize piezoelectric thin films at the nanoscale level.<sup>16</sup>

The PFM technique employs a conducting AFM probe, which is in contact with the surface to locally bias the sample. For piezoelectric materials, this causes detectable surface displacements due to converse piezoactuation. In a typical experiment setup, the piezoelectric thin film is mounted or grown on a conducting substrate that is grounded during the PFM measurement. A bias is applied to the tip from a signal generator, which includes a periodic ac signal ( $V_{ac}$  oscillating at frequency  $\omega$ ). With the AFM probe acting as the top electrode and the conducting substrate as the back electrode, an ac electric field is thereby applied across the piezoelectric film. Any resulting surface displacements beneath the tip are then detected as deflections of the integrated AFM cantilever using a lock-in amplifier. This transduction is achieved by reflecting a laser or light emitting diode beam off the back of the lever onto a position sensitive photodiode. The output measured by the lock-in amplifier gives the piezoresponse in terms of changes in amplitude with respect to the applied ac field. The amplitude data are then plotted as a function of  $x$ - $y$  position of the topography image. At its simplest, the amplitude of sample vibration normal to the surface detected during PFM ( $z_{vibration}$ ) is proportional to the converse piezoelectric coefficient and the ac applied bias  $V_{ac}$  given by the equation

$$z_{vibration} = d_{zz} V_{ac}.$$

As a result, PFM provided piezoresponse data and images reveal the coupling between the electromechanical responses of the sample. In addition, electrostatic forces acting between the probe and the sample as well as forces distributed along the cantilever may also be detected,<sup>17</sup> though these were minimized in the present measurement. In particular, earlier works have shown that PFM carried out at ac frequencies corresponding to contact resonances of the cantilever (1–2 MHz) can result in higher piezoactuation contrast and resolution, a strategy employed in this work.<sup>18–20</sup>

For this paper, PFM data were obtained for the multilayered and homogenous BST samples by acquiring multiple  $5 \mu\text{m}$  scan size images at a single location on each sample ( $256 \times 256$  pixels). No dc voltage was applied at the tip, but the ac voltage was increased image by image from 1 to 10 V (peak to peak) in steps of  $0.5 V_{p.p.}$ . This resulted in sets of 19 images of the same area, each at distinct applied ac biases,

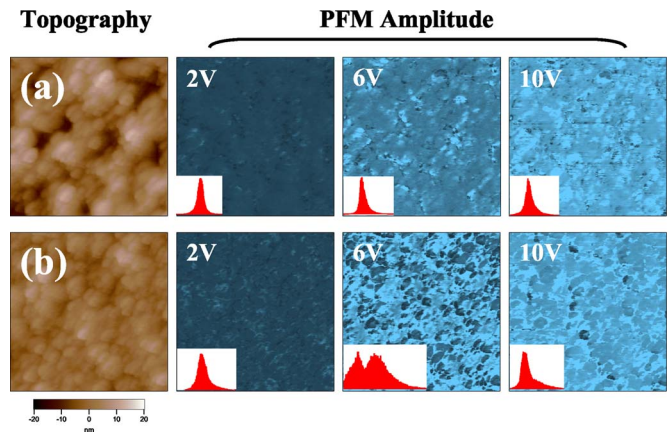


FIG. 2. (Color online) (a) AFM topography and PFM amplitude images ( $5 \times 5 \mu\text{m}^2$ ) taken at 2, 6, and 10  $V_{ac,p.p.}$  for the homogenous BST film. (b) The same image types and conditions obtained for the multilayer graded sample.

for each sample. In order to make a meaningful comparison of the piezoresponse between the two samples, all measurements for both samples were made during a single imaging session and PFM scanning conditions such as equipment offsets and sensitivity as well as the frequency and voltages of the ac field were kept the same throughout. Subsequent measurements at different sample locations yielded equivalent results.

A subset of the AFM images obtained during the measurements for the homogenous and multilayered sample are shown in Figs. 2(a) and 2(b). The surface topography images show that the homogenous and multilayered films have relatively smooth surfaces with root mean square roughness values of 5 and 3 nm, respectively. For the homogenous sample, PFM amplitude images taken at each voltage step exhibit a uniform contrast, with the average amplitude steadily increasing with each incremental step as expected. This is illustrated in Fig. 2(a) for PFM images taken at 2, 6, and 10 V. The overall intensity of the images increases with bias showing the stronger piezoresponse as the ac voltage increases. Histogram data obtained from each of the PFM images (insets) denote Gaussian distributions with single narrow peaks.

For the multilayered films, the PFM image at 2 V shows uniform contrast with a single peak Gaussian distribution, just as observed in the homogenous film. However, as the ac voltage is increased to intermediate voltages such as 6 V, the PFM images begin to exhibit areas of two distinct contrast levels. These spatial inhomogeneities are especially apparent in histogram data from the 6 V PFM image (also inset), which confirm the bimodal distribution of regions with lower and higher piezoresponse. As the voltage is increased beyond 7.5 V, the piezoresponse becomes uniform again with a narrowing, single peak, Gaussian distribution.

The average piezoresponse of each PFM image obtained at distinct ac excitation amplitudes is plotted for both the homogenous and multilayered samples in Fig. 3. For the homogenous sample, the piezoresponse increases linearly with increasing ac voltage from 1 to 10 V as anticipated. For the graded sample, at lower voltages ( $< 2$  V) the piezoresponse is similar for both samples with no obvious enhancement of the piezoelectric strain in the multilayered sample. Both the multilayer and the homogeneous films consist of randomly oriented grains with randomly oriented polarization vectors.

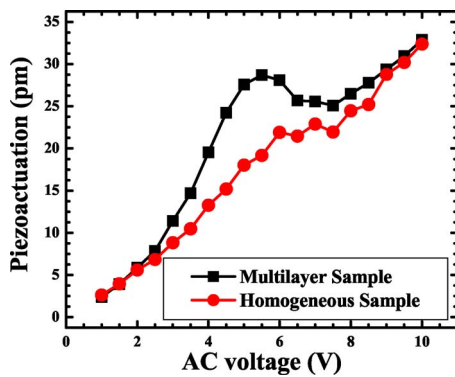


FIG. 3. (Color online) Calculated average piezoresponse of PFM images obtained at each voltage step vs ac voltage for the multilayer and homogeneous samples. 95% confidence error bars are less than 3% and too negligible to be visible on the graph.

However, in the multilayer heterostructure the magnitude of the polarization vector changes from one composition to the other. At small external fields, these random polarization vectors start to align but the applied potential is not strong enough to pole the grains. As the external voltage is increased, there is an enhancement in the piezoresponse for the multilayered sample by as much as 50% compared to the homogeneous sample. While the gradual increase in the piezoelectricity in both samples may indicate a reorientation of the polarization vectors or just an increase in the component of the polarization vector along the external electric field, we attribute the difference between the two samples, i.e., the “hump” in Fig. 3, to the local internal built-in field due to the polarization gradient in the layered ferroelectric film.<sup>21</sup> A straightforward application of Maxwell’s equations relates a spatial variation in polarization to an internal field through  $\nabla E(z) = -(1/\epsilon\epsilon_0)\nabla P(z)$  in a ferroelectric with no free charges and with polarization variations along a  $z$  axis, where  $\epsilon_0$  is the permittivity of free space and  $P(z)$  is the position dependent dielectric polarization (induced and spontaneous). It also follows from basic theory of elasticity that there exists a nonlinear position-dependent strain associated with the polarization gradient given by  $u_T(z) = u_m(z) - Q_{12}(z)P(z)^2$ , where  $u_T$  is the total in-plane strain,  $u_m$  is the misfit of each layer with the underlying substrate, and the last term is the eigenstrain of the ferroelectric phase transformation ( $Q_{12}$  an electrostrictive coefficient). We note that the elastic energy due to bending is neglected since the substrate thickness is much larger than the film thickness. The enhancement in the piezoresponse of the multilayer sample relative to the monolithic BST60/40 is somewhat surprising considering that BST60/40 should have a higher intrinsic piezoelectric effect due to the close proximity of the temperature of measurement (25 °C) to the ferroelectric phase transformation at 5 °C compared to the multilayer sample that contains “harder” ferroelectric compositions BST75/25 and BST90/10. These results suggest that the internal electrostatic and electromechanical potential due to the systematic polarization variation improves piezoelectric response as predicted theoretically.<sup>9</sup> At higher voltages (>5.5 V), it is

observed that the enhanced response of the multilayered sample diminishes and at voltages beyond 7.5 V, the response of the multilayered sample is equivalent to the homogeneous sample. This regression can be explained by considering the induced polarization that depends on the dielectric response. The induced polarization at the “softer” end of the multilayer ferroelectric (BST60/40) is larger than the induced polarization at the BST90/10 end since the dielectric response of BST60/40 is larger than that of BST90/10. As such, at high external fields, the polarization gradient and the commensurate internal potential decrease, resulting in a relatively smaller piezoresponse than for intermediate fields.

In summary, we have shown that multilayered FE films with a systematic variation in the composition (and thus the polarization) have a higher piezoelectric response compared to homogeneous samples for certain field magnitudes. This enhancement is substantial (~50%) even for polycrystalline thin films, despite the fact that the microstructure is laterally inhomogeneous. This indicates that ultimately device properties could be further improved for single-crystal, monodomain, epitaxially graded heterostructures.

The work at UConn was supported by the U.S. Army Research Office through Grant W911NF-05-1-0528 and the UConn Foundation.

- <sup>1</sup>H. M. Christen, E. D. Specht, D. P. Norton, M. F. Chisholm, and L. A. Boatner, *Appl. Phys. Lett.* **72**, 2535 (1998).
- <sup>2</sup>A. Erbil, Y. Kim, and R. A. Gerhardt, *Phys. Rev. Lett.* **77**, 1628 (1996).
- <sup>3</sup>T. Harigai, D. Tanaka, H. Kakemoto, S. Wada, and T. Tsurumi, *J. Appl. Phys.* **94**, 7923 (2003).
- <sup>4</sup>T. Harigai and T. Tsurumi, *Ferroelectrics* **346**, 56 (2007).
- <sup>5</sup>T. Hayashi and T. Tanaka, *Jpn. J. Appl. Phys., Part 1* **34**, 5100 (1995).
- <sup>6</sup>K. P. Jayadevan and T. Y. Tseng, *J. Mater. Sci.: Mater. Electron.* **13**, 439 (2002).
- <sup>7</sup>T. Shimuta, O. Nakagawara, T. Makino, S. Arai, H. Tabata, and T. Kawai, *J. Appl. Phys.* **91**, 2290 (2002).
- <sup>8</sup>M. S. Mohammed, G. W. Auner, R. Naik, J. V. Mantese, N. W. Schubring, A. L. Micheli, and A. B. Catalan, *J. Appl. Phys.* **84**, 3322 (1998).
- <sup>9</sup>S. Zhong, Z. G. Ban, S. P. Alpay, and J. V. Mantese, *Appl. Phys. Lett.* **89**, 142913 (2006).
- <sup>10</sup>N. W. Schubring, J. V. Mantese, A. L. Micheli, A. B. Catalan, and R. J. Lopez, *Phys. Rev. Lett.* **68**, 1778 (1992).
- <sup>11</sup>S. Zhong, S. P. Alpay, M. W. Cole, E. Ngo, S. Hirsch, and J. D. Demaree, *Appl. Phys. Lett.* **90**, 092901 (2007).
- <sup>12</sup>G. H. Haertling, *Am. Ceram. Soc. Bull.* **73**, 93 (1994).
- <sup>13</sup>K. M. Mossi, G. V. Selby, and R. G. Bryant, *Mater. Lett.* **35**, 39 (1998).
- <sup>14</sup>M. W. Cole, P. C. Joshi, M. H. Ervin, M. C. Wood, and R. L. Pfeffer, *Thin Solid Films* **374**, 34 (2000).
- <sup>15</sup>M. W. Cole, E. Ngo, S. Hirsch, J. D. Demaree, S. Zhong, and S. P. Alpay, *J. Appl. Phys.* **102**, 034104 (2007).
- <sup>16</sup>R. Nath, R. E. Garcia, J. E. Blendell, and B. D. Huey, *JOM* **59**, 17 (2007).
- <sup>17</sup>B. D. Huey, C. Ramanujan, M. Bobji, J. Blendell, G. White, R. Szozykiewicz, and A. Kulik, *J. Electroceram.* **13**, 287 (2004).
- <sup>18</sup>C. Harnagea, M. Alexe, D. Hesse, and A. Pignolet, *Appl. Phys. Lett.* **83**, 338 (2003).
- <sup>19</sup>H. Okino, J. Sakamoto, and T. Yamamoto, *Jpn. J. Appl. Phys., Part 1* **42**, 6209 (2003).
- <sup>20</sup>U. Rabe, M. Kopycinska, S. Hirsekorn, J. M. Saldana, G. A. Schneider, and W. Arnold, *J. Phys. D* **35**, 2621 (2002).
- <sup>21</sup>Z. G. Ban, S. P. Alpay, and J. V. Mantese, *Phys. Rev. B* **67**, 184104 (2003).